Supplemental Material: Pore-scale Mixing and the Evolution of Hydrodynamic Dispersion in Porous Media

Alexandre Puyguiraud, Philippe Gouze, and Marco Dentz*
Spanish National Research Council (IDAEA-CSIC), Barcelona, Spain and
Geoscience Montpellier, CNRS, Université de Montpellier, Montpellier, France
(Dated: March 25, 2021)

CONTENTS

I. DIRECT NUMERICAL SIMULATIONS

The numerical flow and transport simulations are performed on the three-dimensional image of a Berea sandstone sample obtained by identifying the connected void phase and the solid phase by processing a X-Ray microtomography image (see for example Gouze *et al.* [1] and references therein)

A. Flow

In the following we summarize the methodology to solve the flow field. The binary images of the geometry are composed of 300^3 regular voxels (cubes) that represent either void or solid. The mesh used for solving flow is obtain by dividing each of the image voxels by 3 in each of the direction so that 1 voxel of the image is represented by 27 cubic cells of size $\Delta x = \Delta y = \Delta z = 1.06 \times 10^{-6}$ m. This discretization level is selected such that flow in the smallest throats are is-represented, see also Gjetvaj *et al.* [2]. Thus, the resulting discretization for the regular grid consists of 900^3 cubic cells. We prescribe pressure boundary conditions at the inlet and outlet, and no-slip conditions at the void-solid interfaces and at the remaining domain boundaries. At the inlet a pressure of 0.1 Pa in set while it is zero at the outlet. We then solve the flow with the SIMPLE algorithm [3] implemented in OpenFOAM [4]. Note that,

* E-mail: marco.dentz@csic.es

in order to minimize boundary effects, twenty layers are added at the inlet and outlet [5]. After convergence, this means, once the residual of the pressure and flow fields between two consecutive steps is below 10^{-5}, we extract the complete velocity field. Velocity values are given at every interface of the mesh in the normal direction to the face. More details are given in Gjetvaj *et al.* [2]. The mean flow speed is 7.78×10^{-7} m/s which corresponds to a Reynolds number of $Re \approx 10^{-5}$, meaning that the flow is laminar and can be described by the Stokes equation. The flow fields used for the simulations at different Péclet numbers are obtained by multiplying this flow field by a constant. The corresponding Reynolds numbers are between $Re \approx 10^{-5}$ for $Pe = 1$ and $Re \approx 1$ for $Pe = 10^5$, which is at the upper limit for which the Stokes assumption is still valid.

B. Random walk particle tracking

The random walk particle tracking simulations are based on the Langevin equations

$$\frac{d\mathbf{x}(t)}{dt} = \mathbf{v}[\mathbf{x}(t)] + \sqrt{2D}\boldsymbol{\xi}(t), \tag{1}$$

where, $\boldsymbol{\xi} = (\xi_1, \xi_2, \xi_3)$ is a Gaussian white noise with zero mean and correlation $\langle \xi_i(t)\xi_j(t')\rangle = \delta(t - t')$. We can then discretize the Langevin equations as the current position $\mathbf{x}(t)$ plus an advective and a diffusive component as

$$\mathbf{x}(t + \Delta t) = \mathbf{x}(t) + \mathbf{v}[\mathbf{x}(t)]\Delta t + \sqrt{2D\Delta t}\boldsymbol{\zeta}(t). \tag{2}$$

The advective term is based on an extension of the Pollock algorithm [6–8]. Originally, the Pollock algorithm assumes a linear variation of velocity within an the mesh cells in each direction. It is widely used in reservoirs and very high porosity structures. However, this linear interpolation causes precision errors in the vicinity of solid surfaces since a linear interpolation is no longer accurate. This is why Mostaghimi *et al.* [7] extended the methodology by introducing different types of quadratic interpolations in the voxels that are in contact with the solid phase. This renders this methodology accurate in low porosity media. This methodology allows to know analytically the position $\mathbf{x}(t)$ of a particle for any t and thus permits splitting the trajectory in small time intervals Δt. The advective and diffusive operators are split on this Δt basis, allowing for the computation of the diffusive jumps between advective steps.

The diffusive jumps are computed following the third term on the right side of equation (2) where $\boldsymbol{\zeta} = (\zeta_1, \zeta_2, \zeta_3)$ with ζ_i being uniform random variables in $[-\sqrt{3}, \sqrt{3}]$ with $\langle \boldsymbol{\zeta}(t)\rangle = \mathbf{0}$ and $\langle \zeta_i(t)\zeta_j(t)\rangle = \delta_{ij}$. The central limit theorem guarantees that the sum of the random motions is Gaussian. Using uniformly generated random variables rather than Gaussian present two main advantages. The computational cost is reduced and there is a better control on the maximum displacement jump that a particle can do. This avoids unexpectedly large displacement that can jump over solid cells and thus, allows for a moderately large Δt.

In order to simulate particle displacement over distances larger than the sample size, we reinject the particles at the inlet boundary of the domain once they reach the outlet of the sample. To ensure continuity of the speed series of each particle, we first compute the particle speed $v(\mathbf{x}_a)$ at position $\mathbf{x}_a$ at the outlet. Then, we identify the pore area $\mathcal{A}_{v(\mathbf{x}_a)}$ at the inlet plane where the speed values $v(\mathbf{x}_b)$ at positions $\mathbf{x}_b \in \mathcal{A}_{v(\mathbf{x}_a)}$ fulfill $v(\mathbf{x}_b) \in [v(\mathbf{x}_a) - \Delta v, v(\mathbf{x}_a) + \Delta v]$, where $\Delta v = v(\mathbf{x}_a)/200$. The particle is then reinjected in a random location within $\mathcal{A}_{v_L(\mathbf{x})}$. This procedure preserves the speed continuity and ensures that no artificial decorrelation is occurring. Besides, in the case of a particle exiting the domain through the inlet, by diffusion, the particle is reinjected at the outlet following a similar procedure.

II. SPEED DISTRIBUTIONS

We derive here the distribution of the mean flow speeds and then of the particle speeds that is required in the time-domain random walk approach.

A. Mean flow speeds

We conceptualize the porous medium as a network of conducts and joints. Within each conduct, the volumetrically sampled speed distribution is uniform,

$$p(v|v_m) = \frac{1}{2v_m} H(2v_m - v), \tag{3}$$

where v_m is the mean speed in the conduct. The Eulerian speed distribution $p_e(v)$ is constructed by integration of $p(v|v_m)$ over all conducts weighted by the distribution $p_m(v)$ of mean speeds. This gives

$$p_e(2v) = \int_v^\infty dv_m p_m(v_m) \frac{1}{2v_m}. \tag{4}$$

This implies that the distribution of mean pore speeds can be obtained from the Eulerian speed PDF as

$$p_m(v) = -2v \frac{dp_e(2v)}{dv}. \tag{5}$$

B. Particle speeds

In the time-domain random walk, the partitioning of particles at turning points (the joints) is proportional to the flow rate into the downstream conducts. In our model, the distribution of Eulerian speeds and thus mean speeds is obtained through volumetric sampling within the void space of the porous medium,

$$p_m(v) = \frac{1}{V_0} \sum_p V_p \delta(v - v_p). \tag{6}$$

The distribution $p_s(v)$ of speeds is weighted by the flow rate of the conducts, which means

$$p_s(v) = \frac{1}{\sum_p A_p v_p} \sum_p A_p v_p \delta(v - v_p). \tag{7}$$

We assume that the length of the conducts is approximately constant such that $V_p = A_p \ell_0$. Thus, we can write

$$p_s(v) = \frac{1}{\sum_p V_p v_p} \sum_p V_p v_p \delta(v - v_p) = \frac{v}{\langle v_e \rangle} p_e(v). \tag{8}$$

III. TRANSITION TIME DISTRIBUTION

We first derive the distribution of transition times for a single conduct, and then the compound transition time distribution on the network scale.

A. Single Conduct

The transition time distribution for a single conduct is obtained from the solution of the following first-passage problem. We consider an instantaneous injection of tracer at the upstream turning point at $x = 0$, and an absorbing boundary at the downstream turning point at $x = \ell_v$. This means

$$\frac{\partial g(x,t)}{\partial t} + v \frac{\partial g(x,t)}{\partial x} - D \frac{\partial^2 g(x,t)}{\partial x^2} = 0 \tag{9}$$

with the boundary conditions

$$v g(x,t) - D \frac{g(x,t)}{\partial x} = \delta(t), \qquad x = 0, \tag{10}$$

$$g(x,t) = 0, \qquad x = \ell_v, \tag{11}$$

and the initial condition $g(x, t = 0) = 0$. The first passage time distribution over the downstream boundary is given by

$$\psi_0(t|v) = -D \frac{\partial g(x,t)}{\partial x}\bigg|_{x=\ell_v}. \tag{12}$$

We solve this first passage problem in Laplace space. Laplace transform of (9) gives

$$\lambda g^*(x,\lambda) + v\frac{\partial g^*(x,\lambda)}{\partial x} - D\frac{\partial^2 g^*(x,\lambda)}{\partial x^2} = 0. \tag{13}$$

The solution is given by

$$g^*(x,\lambda) = A(\lambda)\exp(Pe_v x/\ell_v)\sinh\left[\frac{\ell_v - x}{\ell_v}B(\lambda)\right], \qquad B(\lambda) = \sqrt{Pe_v^2 + \lambda\tau_D}, \tag{14}$$

where we defined $Pe_v = v\ell_v/2D$. The constant $A(\lambda)$ is determined from the boundary condition at 0,

$$vg^*(x,\lambda) - D\frac{g^*(x,\lambda)}{\partial x} = 1, \qquad x = 0. \tag{15}$$

Inserting (14) into the latter gives

$$A = \frac{\ell_v/D}{Pe_v\sinh(B) + B\cosh(B)}. \tag{16}$$

Thus, we obtain $g^*(x,\lambda)$

$$g^*(x,\lambda) = \frac{\ell_v}{D}\frac{\exp(Pe_v x/\ell_v)\sinh\left[\frac{\ell_v - x}{\ell_v}B(\lambda)\right]}{Pe_v\sinh(B) + B\cosh(B)}. \tag{17}$$

This gives for the first passage time distribution

$$\psi_0^*(\lambda|v) = \frac{B\exp(Pe_v)}{Pe_v\sinh(B) + B\cosh(B)}. \tag{18}$$

1. *Moments*

The mean travel time is defined by

$$\langle\tau|v\rangle = -\left.\frac{df^*(\lambda)}{d\lambda}\right|_{\lambda=0}. \tag{19}$$

We obtain

$$\langle\tau|v\rangle = \tau_v\left[1 - \frac{\exp(-Pe_v)\sinh(Pe_v)}{Pe_v}\right], \tag{20}$$

where we defined $\tau_v = \ell_v/v$. The mean squared travel time is defined by

$$\langle\tau^2|v\rangle = \left.\frac{d^2 f^*(\lambda)}{d\lambda^2}\right|_{\lambda=0}. \tag{21}$$

We obtain

$$\langle\tau^2|v\rangle = \tau_v^2\left(1 - \frac{1}{Pe_v^2} + \frac{\exp(-2Pe_v)}{Pe_v}\left[3 + \frac{1}{2Pe_v} + \frac{\exp(-2Pe_v)}{2Pe_v}\right]\right). \tag{22}$$

2. *Numerical Approximation*

Numerically, we approximate $\psi_0(t|v)$ by the truncated inverse Gaussian distribution

$$G(t) = \frac{\exp\left[-\frac{\tau_v^{-2}(t-\tau_v)^2}{4t/\tau_D}\right]}{t\sqrt{4\pi t/\tau_D}}\exp(-kt - Pe_v + \sqrt{Pe_v^2 + k\tau_D}). \tag{23}$$

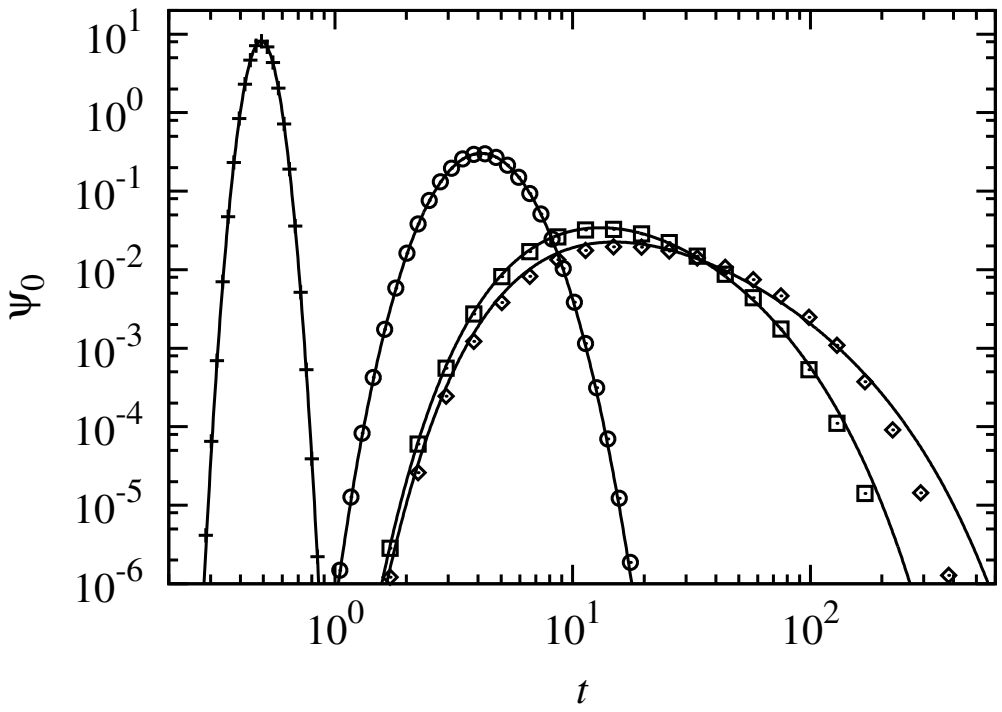

Figure 1. First passage time distribution $\psi_0(t|v)$ obtained from numerical inverse Laplace transform of (18) for local Péclet numbers of (crosses) $Pe_v = 10^2$ (circles) 10, (squares) 1 and (diamonds) 10^{-1}. The solid lines denote the corresponding approximations by the truncated inverse Gaussian distribution (23).

The constant k is chosen such that $G(t)$ has the same mean transition time as $\psi_0(t|v)$. It is determined as follows. The Laplace transform of $G(t)$ is given by

$$G^*(\lambda) = \exp\left[-\sqrt{Pe_v^2 + (\lambda + k)\tau_D} + \sqrt{Pe_v^2 + k\tau_D}\right]. \tag{24}$$

The first moment is given by

$$m_G = \frac{\tau_D}{2\sqrt{Pe_v^2 + k\tau_D}} \equiv \langle \tau|v\rangle. \tag{25}$$

Thus, we obtain for k

$$k\tau_D = \frac{\tau_D^2}{4\langle\tau|v\rangle^2} - Pe_v^2 = Pe_v^2\left(\frac{\tau_v^2}{\langle\tau|v\rangle^2} - 1\right). \tag{26}$$

Figure 1 shows the first passage time distribution and the approximation by the truncated inverse Gaussian distribution. Random numbers are sampled numerically from the truncated inverse Gaussian distribution by using the algorithm of Michael *et al.* [9] for the inverse Gaussian random variable in combination with rejection sampling in order to account for the exponential cutoff.

B. Network scale

We first analyze the behavior of the transition time distribution and specifically its behavior for times smaller and larger than τ_D. Then, we consider the behavior of the mean and of the mean squared travel time for large Péclet numbers.

The transition time distribution $\psi(t)$ for the network of conducts is obtained for $\psi_0(t|v)$ and $p_m(v)$ as

$$\psi(t) = \int_0^\infty dv \frac{v}{\langle v_m\rangle} p_m(v)\psi_0(t|v). \tag{27}$$

For $Pe_v \gg 1$, that is for $v \gg D_m/\ell_v$ $\psi_0(t|v)$ is sharply peaked about $\tau_v = \ell_v/v$, while for $Pe_v \ll 1$, that it $v \ll D_m/\ell_v$ it is $\psi_0(t|v) = \psi_0(t)$ independent of v and a function of τ_D only. Thus, we can approximate

$$\psi(t) \approx \int_{D_m/\ell_v}^{\infty} dv \frac{v}{\langle v_m \rangle} p_m(v) \delta(t - \ell_v/v) + \int_0^{D_m/\ell_v} dv \frac{v}{\langle v_m \rangle} p_m(v) \psi_0(t). \tag{28}$$

This gives

$$\psi(t) \approx \frac{\ell_v}{\langle v_m \rangle t^3} p_m(\ell_v/t) H(\tau_D - t) + C\psi_0(t), \tag{29}$$

with C a constant. Thus, for times $t \ll \tau_D$, the transition time distribution is dominated by the speed distribution $p_m(v)$, and for time $t \gg \tau_D$ by the diffusive cut-off τ_D.

In the following, we consider speed distributions that behave as the power-law

$$p_m(v) \sim v^{-1-\alpha} \tag{30}$$

for $v \ll v_0$ with v_0 a characteristic velocity, and which decay exponentially fast for $v \gg v_0$. For illustration one can think of a Gamma distribution. The transition time distribution thus behaves as

$$\psi(t) \sim t^{-2-\alpha} \tag{31}$$

for $t \ll \tau_D$.

The mean travel time is given by

$$\langle \tau \rangle = \int_0^{\infty} dv \frac{v}{\langle v_m \rangle} p_m(v) \langle \tau | v \rangle. \tag{32}$$

Inserting expression (20) gives

$$\langle \tau \rangle = \tau_v \left[1 - \int_0^{\infty} dv p_m(v) \frac{\exp(-Pe_v) \sinh(Pe_v)}{Pe_v} \right]. \tag{33}$$

Next, we rescale the integration variable as $v \to v/v_m$, which gives

$$\langle \tau \rangle = \tau_v \left[1 - \int_0^{\infty} dv \hat{p}_m(v) \frac{\exp(-Pe_c v) \sinh(Pe_c v)}{Pe_c v} \right], \tag{34}$$

where we defined $Pe_c = \langle v_m \rangle \ell_v / 2D_m$ and $\hat{p}_m(v) = \langle v_m \rangle p_m(\langle v_m \rangle v)$. Note that $Pe_c = Pe\ell_v/\ell_0$. The leading order behavior of $\langle \tau \rangle$ for $Pe_c \gg 1$ is

$$\langle \tau \rangle = \tau_v + \ldots, \tag{35}$$

where the dots denote contributions of order Pe.

The mean squared travel time is

$$\langle \tau^2 \rangle = \int_0^{\infty} dv \frac{v}{\langle v_m \rangle} \tau_v^2 p_m(v) F(Pe_v) = \int_0^{\infty} dv \frac{\ell_v^2}{v \langle v_m \rangle} p_m(v) F(Pe_v) = \tau_v^2 \int_0^{\infty} dv \frac{\langle v_m \rangle}{v} p_m(v) F(Pe_v), \tag{36}$$

where we defined $\langle \tau^2 | v \rangle = \tau_v^2 F(Pe_v)$. We note that $F(Pe_v)$ behaves for $Pe_v \ll 1$ as $F(Pe_v) = 5Pe_v^2/3$ and is equal to 1 in the limit $Pe_v \to \infty$. Next, we rescale the integration variable as $v \to v/v_m$. This gives

$$\langle \tau^2 \rangle = \tau_v^2 \int_0^{\infty} dv \frac{1}{v} \hat{p}_m(v) F(vPe_c). \tag{37}$$

The mean of $\hat{p}_m(v)$ is equal to 1. If

$$\int_0^\infty dv v^{-1}\hat{p}_m(v) < \infty, \tag{38}$$

this means if $\hat{p}_m(v)$ goes to 0 for $v \to 0$, the mean squared transition time behaves as

$$\langle \tau^2 \rangle \sim \tau_v^2 \tag{39}$$

in leading order for $Pe_c \gg 1$. If $\hat{p}_m(v)$ has an integrable singularity at 0, this means, if $\hat{p}_m(v) \sim v^{\alpha-1}$ with $0 < \alpha \leq 1$, we rescale the integration variable as $v \to vPe_c$. This gives

$$\langle \tau^2 \rangle = \tau_v^2 \int_0^\infty dv \frac{1}{v}\hat{p}_m(v/Pe_c)F(v). \tag{40}$$

We set $\hat{p}_m(v) = v^{\alpha-1}\varphi(v)$, where $\varphi(v)$ goes toward a constant for $v \to 0$ and decays exponentially fast for $v \to \infty$. For illustration, one may think of a Gamma distribution with mean 1. Thus, we obtain

$$\langle \tau^2 \rangle = \tau_v^2 Pe_c^{1-\alpha} \int_0^\infty dv v^{\alpha-2}\varphi(v/Pe_c)F(v). \tag{41}$$

For $0 < \alpha < 1$, the leading order behavior in the limit of large $Pe_c \gg 1$ is

$$\langle \tau^2 \rangle \sim \tau_v^2 Pe_c^{1-\alpha}. \tag{42}$$

For $\alpha = 1$, we can write

$$\langle \tau^2 \rangle = \tau_v^2 \int_0^\infty dv \frac{1}{v}\varphi(v/Pe_c)F(v) \approx \tau_v^2 \int_0^{Pe_v} dv \frac{1}{v}F(v), \tag{43}$$

because $\varphi(v/Pe_c)$ sets a cutoff at Pe_c. Since $F(v) \to 1$ for $v \gg 1$, we obtain in leading order

$$\langle \tau^2 \rangle = \tau_v^2 \ln(Pe_c). \tag{44}$$

IV. IMPLEMENTATION OF THE STOCHASTIC TIME-DOMAIN RANDOM WALK MODEL

The numerical simulations of the derived stochastic particle model is based on the equations of motion

$$x_{n+1} = x_n + \ell_v/\chi, \qquad t_{n+1} = t_n + \tau_n. \tag{45}$$

The time increments τ_n are generated as follows. A speed v is sampled according to the distribution $p_s(v)$ by inverse sampling. Then, the transition time is obtained by sampling from $\psi_0(t|v)$ approximated by the truncated inverse Gaussian distribution (23).

The displacement variance is determined as

$$\sigma^2(t) = \langle x_{n_t}^2 \rangle - \langle x_{n_t} \rangle^2, \tag{46}$$

where $n_t = \max(n|t_n \leq t)$. The first passage time distributions are determined as

$$t_a = \sum_{n=1}^{n_c-1} \tau_n + \tau_{n_c} \frac{x\chi - s_n}{\ell_v}, \tag{47}$$

where $n_c = \lceil \chi x/\ell_v \rceil$. The interpolation for the last step is negligible for $n_c \gg 1$.

V. CONTINUOUS TIME RANDOM WALKS

The continuous time random walk framework [10, 11] gives for the evolution equation of the particle distribution $p(x,t)$ in the derived stochastic time-domain random walk model, the following set of equations,

$$p(x,t) = \int_0^t dt' R(x,t') \int_{t-t'}^{\infty} dt'' \psi(t''), \tag{48}$$

$$R(x,t) = \delta(x)\delta(t) + \int_0^t dt R(x - \ell_v/\chi, t')\psi(t-t'). \tag{49}$$

These equations can be solved for the Fourier-Laplace transform $\tilde{p}^*(k,\lambda)$ of $p(x,t)$ [12], which gives

$$\tilde{p}^*(x,\lambda) = \frac{1}{\lambda}\frac{1-\psi^*(\lambda)}{1-\exp(ik\ell_v/\chi)\psi^*(\lambda)}. \tag{50}$$

The Fourier transform is defined here as

$$\tilde{\varphi}(k) = \int_{-\infty}^{\infty} dx \exp(ikx)\varphi(x), \qquad \varphi(x) = \int_{-\infty}^{\infty} \frac{dk}{2\pi} \exp(-ikx)\tilde{\varphi}(k). \tag{51}$$

The first and second displacement moments are defined in terms of $\tilde{p}^*(k,\lambda)$ as

$$m_1^*(\lambda) = -i \left.\frac{\partial \tilde{p}^*(k,\lambda)}{\partial k}\right|_{k=0} \tag{52}$$

$$m_2^*(\lambda) = - \left.\frac{\partial^2 \tilde{p}^*(k,\lambda)}{\partial k^2}\right|_{k=0}. \tag{53}$$

Using expression (50), we obtain [12]

$$m_1^*(\lambda) = v_0 \lambda^{-2} \mathcal{K}^*(\lambda), \tag{54a}$$

$$m_2^*(\lambda) = 2D_0\lambda^{-2}\mathcal{K}^*(\lambda) + 2v_0^2\lambda^{-3}\mathcal{K}^*(\lambda)^2, \tag{54b}$$

where we defined

$$\mathcal{K}^*(\lambda) = \frac{\langle\tau\rangle\lambda\psi^*(\lambda)}{1-\psi^*(\lambda)}, \tag{55}$$

and

$$v_0 = \frac{\ell_v}{\chi\langle\tau\rangle}, \qquad D_0 = \frac{\ell_v^2}{2\chi^2\langle\tau\rangle}. \tag{56}$$

A. Asymptotic transport

In order to determine the asymptotic large scale transport properties, we expand the kernel (55) up to linear order in λ

$$\mathcal{K}^*(\lambda) = 1 + \lambda\mathcal{K}^\infty, \qquad \mathcal{K}^\infty = \frac{1}{2}\frac{\langle\tau^2\rangle - 2\langle\tau\rangle^2}{\langle\tau\rangle}. \tag{57}$$

Thus, we obtain for (54)

$$m_1^*(\lambda) = v_0\lambda^{-2}(1+\lambda\mathcal{K}^\infty), \tag{58}$$

$$m_2^*(\lambda) = 2D_0\lambda^{-2}(1+\lambda\mathcal{K}^\infty) + 2v_0^2\lambda^{-3}(1+\lambda\mathcal{K}^\infty)^2. \tag{59}$$

Inverse Laplace transform gives

$$m_1(t) = v_0(t + \mathcal{K}^\infty) \tag{60a}$$

$$m_2(t) = 2D_0(t + \mathcal{K}^\infty) + v_0^2(t + \mathcal{K}^\infty)^2 + 2v_0^2\mathcal{K}^\infty t + \mathcal{K}^{\infty 2}. \tag{60b}$$

The mean velocity and hydrodynamic dispersion coefficient are defined by

$$v_\infty = \frac{d}{dt} m_1(t) \tag{61}$$

$$D^* = \frac{1}{2}\frac{d}{dt}\left[m_2(t) - m_1(t)^2\right]. \tag{62}$$

Using (60), we obtain

$$v_\infty = v_0 \tag{63}$$

$$D^* = D_0 + v_0^2 \frac{1}{2}\frac{\langle\tau^2\rangle - 2\langle\tau\rangle^2}{\langle\tau\rangle} = D_0\left(1 + \frac{\langle\tau^2\rangle - 2\langle\tau\rangle^2}{\langle\tau\rangle^2}\right) = D_0\frac{\sigma_\tau^2}{\langle\tau\rangle^2}. \tag{64}$$

1. *Tortuosity*

The macroscopic transport velocity is equal to the mean pore velocity $v_\infty = \overline{u}$ [13]. Thus, we obtain from (63) with (56) that the tortuosity is given by

$$\chi = \frac{\ell_v}{\overline{u}\langle\tau\rangle}. \tag{65}$$

Using (33) gives the explicit expression

$$\chi = \chi_a\left[1 - \int_0^\infty dv p_m(v)\frac{\exp(-Pe_v)\sinh(Pe_v)}{Pe_v}\right]^{-1}, \tag{66}$$

where $\chi_a = \langle v_e\rangle/\overline{u}$.

2. *Hydrodynamic dispersion coefficient*

Equation (65) together with (56) in (64) gives for the hydrodynamic dispersion coefficient

$$D^* = \overline{u}^2\frac{\sigma_\tau^2}{2\langle\tau\rangle}. \tag{67}$$

The full Péclet dependence of D^* can be obtained by using expressions (33) and (36) for the mean and mean squared transition times.

We determine now the leading order behavior of D^* for $Pe_c \gg 1$. For $0 < \alpha < 1$, we obtain by using (35) and (42)

$$D^* \sim \overline{u}^2\tau_v Pe_c^{1-\alpha} = \langle v_m\rangle\ell_v\chi_a^{-2}, Pe_c^{1-\alpha} \tag{68}$$

and therefore

$$D^*/D_m \sim Pe_c^{2-\alpha}. \tag{69}$$

Similarly, we obtain for $\alpha = 1$ by using (44)

$$D^* \sim \overline{u}^2\tau_v \ln(Pe_c) = \langle v_m\rangle\ell_v\chi_a^{-2}\ln(Pe_c), \tag{70}$$

and thus

$$D^*/D_m \sim Pe_c\ln(Pe_c). \tag{71}$$

For $\alpha > 1$, we obtain by using (39)

$$D^* \sim \overline{u}^2\tau_v = \langle v_m\rangle\ell_v\chi_a^{-2}, \tag{72}$$

and thus

$$D^*/D_m \sim Pe_c. \tag{73}$$

B. Anomalous dispersion

Anomalous dispersion is measured by the displacement variance $\sigma^2(t) = m_2(t) - m_1(t)$. The first and second displacement moments $m_1(t)$ and $m_2(t)$ are given in Laplace space by (54). At times $t \ll \tau_D$, the transition time distribution behaves as $\psi(t) \sim t^{-2-\alpha}$. For $0 < \alpha < 1$, its Laplace transform can be expanded as

$$\psi^*(\lambda) = 1 - \lambda\langle\tau\rangle + b\lambda^{1+\alpha}, \tag{74}$$

with b a constant. Inserting this expansion into (55), we obtain in leading order for $\mathcal{K}(\lambda)$

$$\mathcal{K}(\lambda) = 1 + b\lambda^{\alpha}/\langle\tau\rangle. \tag{75}$$

Thus, we obtain for $m_1^*(\lambda)$

$$m_1^*(\lambda) = v_0\lambda^{-2} + b\lambda^{\alpha-2}/\langle\tau\rangle \tag{76}$$

This implies

$$m_1(t) = v_0 t + \ldots, \tag{77}$$

where the dots denote subleading contributions of order $t^{1-\alpha}$. For the second moment, we obtain

$$m_2^*(\lambda) = 2D_0\lambda^{-2} + 2v_0^2\lambda^{-3} + 2bv_0^2\lambda^{\alpha-3}/\langle\tau\rangle, \tag{78}$$

Inverse Laplace transform gives

$$m_2(t) = 2D_0 t + v_0^2 t^2 + 2v_0^2 b t^{2-\alpha}/\langle\tau\rangle\Gamma(1-\alpha). \tag{79}$$

Thus, we obtain for the displacement variance

$$\sigma^2(t) \sim t^{2-\alpha}. \tag{80}$$

For $\alpha = 1$, the Laplace transform of $\psi(t)$ can be expanded as

$$\psi^*(\lambda) = 1 - \langle\tau\rangle\lambda - c\lambda^2\ln(\lambda), \tag{81}$$

with c a constant. Inserting this expansion into (55), we obtain in leading order for $\mathcal{K}(\lambda)$

$$\mathcal{K}(\lambda) = 1 - c\lambda\ln(\lambda)/\langle\tau\rangle. \tag{82}$$

Thus, we obtain for $m_1^*(\lambda)$

$$m_1^*(\lambda) = v_0\lambda^{-2} + \ldots \tag{83}$$

This implies

$$m_1(t) = v_0 t + \ldots, \tag{84}$$

where the dots denote subleading contributions. For the second moment, we obtain

$$m_2^*(\lambda) = 2D_0\lambda^{-2} + 2v_0^2\lambda^{-3} - 2v_0^2 c\lambda^{-2}\ln(\lambda)/\langle\tau\rangle. \tag{85}$$

Inverse Laplace transform gives

$$m_2(t) = 2D_0 t + v_0^2 t^2 + 2v_0^2 c' t\ln(t)/\langle\tau\rangle, \tag{86}$$

with c' a constant. Thus, we obtain for the displacement variance

$$\sigma^2(t) \sim t\ln(t). \tag{87}$$

---

[1] P. Gouze, Y. Melean, T. Le Borgne, M. Dentz, and J. Carrera, Water Resources Research **44** (2008), 10.1029/2007WR006690.

[2] F. Gjetvaj, A. Russian, P. Gouze, and M. Dentz, Water Resources Research **51**, 8273 (2015).
[3] S. V. Patankar, *Numerical Heat Transfer and Fluid Flow* (Hemisphere Publishing Corporation, 1980).
[4] H. G. Weller, G. Tabor, H. Jasak, and C. Fureby, Computers in physics **12**, 620 (1998).
[5] R. Guibert, P. Horgue, G. Debenest, and M. Quintard, Mathematical Geosciences , 1 (2015).
[6] D. W. Pollock, Ground Water **26**, 743 (1988).
[7] P. Mostaghimi, B. Bijeljic, and M. Blunt, Mathematical Geosciences , 1131 (2012).
[8] A. Puyguiraud, P. Gouze, and M. Dentz, Water Resources Research **55** (2019), 10.1029/2018WR023702.
[9] J. R. Michael, W. R. Schucany, and R. W. Haas, The American Statistician **30**, 88 (1976).
[10] H. Scher and M. Lax, Phys. Rev. B **7**, 4491 (1973).
[11] B. Berkowitz, A. Cortis, M. Dentz, and H. Scher, Reviews of Geophysics **44** (2006).
[12] M. F. Shlesinger, Journal of Statistical Physics **10**, 421 (1974).
[13] J. Bear, *Dynamics of fluids in porous media* (American Elsevier, New York, 1972).